Incorporation of bioactive peptides into peptide nanofibrillar hydrogels affects their nanostructure, mechanical properties and biocompatibility

Christopher J.H. Chong[a], Mirren Charnley[b,c,d] Julian Ratcliffe[e], Lilith M. Caballero-Aguilar[f,g], Simon E. Moulton[f,g,h], Katrina J. Binger[a], Nicholas P. Reynolds[a*]

a Department of Biochemistry & Chemistry, La Trobe Institute for Molecular Science, La Trobe University, Bundoora, Victoria 3083, Australia

b Centre for Optical Sciences, Faculty of Science Engineering and Technology, Swinburne University of Technology, Hawthorn, Victoria 3122, Australia

c Immune Signalling Laboratory, Peter MacCallum Cancer Centre, Parkville, Victoria 3000, Australia

d Department of Health Sciences and Biostatistics, Swinburne University of Technology, Hawthorn, Victoria 3122, Australia

e La Trobe University Bioimaging Platform, La Trobe University, Bundoora, Victoria 3083, Australia

f Aikenhead Centre for Medical Discovery, St Vincent's Hospital, Fitzroy, Victoria 3065, Australia

g ARC Centre of Excellence for Electromaterials Science, School of Science, Computing and Engineering Technologies, Department of Engineering Technologies, Swinburne University of Technology, Victoria 3122, Australia

h Iverson Health Innovation Research Institute, Swinburne University of Technology, Hawthorn, Victoria 3122, Australia

* Corresponding author: nicholas.reynolds@latrobe.edu.au

Abstract

Ultrashort self-assembling peptides of typically less than 5 amino acids in length can be modified with highly aromatic protecting groups such as Fluorenylmethyloxycarbonyl (Fmoc) resulting in the rapid formation of nanofibrillar hydrogels. These hydrogels show great promise as scaffolds for tissue engineering and 3D cell culture. If further modified with bioactive peptide sequences, the hydrogels can be used to promote and control cell adhesion, and even support the ability for cultured mesenchymal stem cells (MSCs) to differentiate into therapeutically useful lineages, such as chondrocytes. Whilst there have been numerous examples of how the addition of such sequences can promote the bioactivity of cultured cells, the effect adding these sequences has on the nanoarchitecture, mechanical properties and stability of the resultant hydrogels is less well explored. Here, we have performed a series of experiments investigating the effect incorporating stoichiometric amounts of Fmoc-Arg-Gly-Asp (Fmoc-RGD) into Fmoc-Phe-Phe (Fmoc-FF) hydrogels has on nanofibril morphology, and the rheological properties and stability of the formed gels. Furthermore, we correlate these variations in nano-architectural and mechanical properties with their ability to support the culture of clinically valuable bone marrow derived human mesenchymal stem cells (hMSCs). Our results show that at relatively low concentrations Fmoc-RGD is incorporated into the self-assembled Fmoc-FF nanofibrils creating biocompatible hydrogels capable of supporting hMSC growth for up to a week. At increased concentrations of Fmoc-RGD, incorporation into the nanofibrils is lost and the hydrogels that form are no longer stable enough to support the culture of hMSCs for multiple days. These findings shed light on the importance of balancing the positive effects of adding bioactive ligands to 3D scaffolds with the negative effects these ligands can have on the stability and mechanical properties of these scaffolds. Further, the findings will have implications for the choice of ultrashort peptide scaffolds for tissue engineering applications to support MSCs towards chondrogenic differentiation, and their application as gel-cell constructs in cartilage tissue engineering for osteoarthritis.

Keywords: *Fmoc-FF, Fmoc-RGD, scaffolds, hydrogels, mesenchymal stem cells, ultrashort peptides, self-assembly, nanofibrils*

1. INTRODUCTION

Osteoarthritis (OA) is a degenerative joint condition characterised by destruction of articular cartilage and joint inflammation. Global Burden of Disease data estimated 303.1 million cases of hip and knee OA worldwide in 2017, and with age-standardised prevalence, incidence and years lived with disability rising incrementally by 8-10 % since 1990 [1]. The socioeconomic burden of the disease is similarly significant, with an estimated 1-2.5 % of gross domestic product (GDP) in high income countries attributed to related treatment costs [2]. Sufferers themselves typically experience issues of debilitating pain, loss of mobility and difficulties maintaining functional independence. Current surgical interventions to treat or prevent OA are problematic, [3] leading to high failure rates and / or poor outcomes [4, 5]. Mesenchymal stem cells (MSCs) are a promising cellular therapeutic to restore cartilage loss that occurs in OA. Their potential to self-replicate, differentiate into chondrocytes, and be recruited from accessible reservoirs within human bone marrow, adipose tissue, synovia and periosteum make them ideal candidates for tissue engineering [6-8]. Direct injection of MSCs into the affected joint is the most common method, but the benefits from this delivery are generally diminished due to poor localisation of cells (engraftment efficiency) [9, 10], limited cell viability [11, 12], and patients' experiences of inflammation, pain and swelling [13, 14].

Injectable biomaterial scaffolds have been increasingly paired with MSC therapies and overcome some of these repair limitations. A well-suited scaffold for cartilage tissue engineering should promote cartilage regeneration through accurate mimicry of chemical and biophysical properties of cartilage extracellular matrix (ECM)[15] , and hold a porous architecture which can allow the passage of nutrients and waste products to synovial fluid in vivo [16]. There are three main groups of scaffolds available: natural polymers (including de-cellularised extracellular matrix (dECM)), synthetic polymers and bioinspired self-assembling peptides. dECM and natural polymers (such as collagen [17, 18], chitosan [19, 20], hyaluronic acid (HA) [19-23]) are the closest available mimics of native tissue with strong similarities in composition, microstructure and biomechanical properties [24]. However, their implementation is limited by diminished tuneable properties, uncontrollable rates of degradation [25], batch-to-batch variation [26], microbial contamination, and xeno-contamination from non-native species upon transplantation [27]. Synthetic polymer scaffolds are attractive due to their ease of synthesis, greater tuneability, higher purity and reduced batch-to-batch variance [28]; however they generally lack the biomimetic nanofibrillar architecture of the ECM. Bioinspired self-assembled peptides combine the advantages of synthetic polymers with a nanofibrillar internal structure that more closely mimics that of the ECM of many tissues [29, 30].

Fluorenylmethyloxycarbonyl (Fmoc) protected peptides are a family of self-assembling peptides that show promise as building blocks for biocompatible hydrogels [31]. The highly aromatic Fmoc protecting

group undergoes pi-pi (π-π) stacking interactions with adjacent Fmoc molecules, enhancing long range order and promoting rapid gelation [32]. The dipeptide motif phenylalanine-phenylalanine (FF) is also a promising peptide for applications in bionanotechnology, as it has been shown to self-assemble into β-sheet rich nanofibrils which mimic the morphology and architecture of the nanofibrillar proteins within the ECM [32-34]. Similar β-sheet nanofibril arrangements have previously been shown to promote cell attachment [35-37] and stem cell differentiation [38, 39]. Fmoc-FF based gels are especially appealing candidates for tissue engineering applications, as they have been shown to readily form stable, transparent and biocompatible hydrogels [40].

Biochemical functionality can be added to hydrogels by introducing bioinspired functional peptide motifs such as arginine-glycine-aspartic acid (RGD) [26, 41-43]. The RGD sequence is found within ECM proteins such as fibronectin, and provides specific molecular binding sites for integrins on membranes of adherent cells; in doing so it facilitates greater cell adhesion, improved cell function and tissue regeneration [44]. Hybrid Fmoc-FF, Fmoc-RGD hydrogels have already shown promise for cartilage tissue engineering. When used to encapsulate MSCs, these gels have shown ability to support cellular multi-differentiation *in vitro* and *in vivo*, with MSCs surviving up to 7 days [42]. The RGD motif has also successfully been implemented to functionalise polyethylene glycol (PEG) [45] and HA hydrogels [46], with their presence contributing towards more robust chondrogenesis, greater sulphated glycosaminoglycan (GAG) production and higher chondrogenic gene expression [45-47]. Despite these encouraging results, little work has been done to optimise the concentration of bioactive ligands in these scaffolds. Just as optimising the physical properties of materials can have large effects of MSC responses,[48, 49] optimising the concentration of bioactive ligands is equally important. For instance, Faia-Torres *et. al.*[50] showed that an optimum surface concentration of (RGD-containing) fibronectin evidently promotes collagen production in differentiating MSCs (production of collagen is a marker for both osteo and chondrogenic differentiation), whilst this effect is diminished or lost at higher concentrations . Furthermore, the overall effect of RGD incorporation on the biophysical properties of the assembled Fmoc-FF nanofibrils is largely unknown. Specifically, how elevating RGD concentration affects factors such as the mechanical properties and biodegradability of gels remains unexplored.

In this work we have characterised the biophysical properties of Fmoc-FF hydrogels with stoichiometric amounts of Fmoc-RGD added pre-gelation (**figure 1**). We used a variety of nanoanalytical and statistical techniques) to determine the biodegradation times, nanofibrillar architectures, and mechanical properties of materials at both a nano- and meso- scale. Our findings are expected to have direct implications for optimising the concentration of bioactive moieties such as RGD in short peptide scaffolds for cartilage tissue engineering.

MATERIALS and METHODS

2.1 Fmoc-FF and Fmoc-FF, Fmoc-RGD Hydrogel Formation.

Fmoc-FF hydrogels were formed from a stock solution of Fmoc-FF (Bachem Ltd., Switzerland, purity > 95 %) dissolved in DMSO (100 mg/mL). The stock solution was diluted in Milli-Q® (MQ) ultrapure water to a final concentration of 5.0 mg/mL. The resulting solution was briefly vortexed and allowed to gelate over a 24 hour period. Hybrid Fmoc-FF Fmoc-RGD hydrogels were formed at 5.0 mg/mL by combining stock solutions of Fmoc-FF and Fmoc-RGD (GL Biochem, China, purity > 95 %) (100 mg/mL in DMSO) in appropriate ratios, and diluting into ultrapure water as above. Three hydrogels were formed at the following ratios:

- 100 % Fmoc-FF, 0 % Fmoc-RGD
- 99 % Fmoc-FF, 1 % Fmoc-RGD
- 95 % Fmoc-FF, 5 % Fmoc-RGD.

For simplicity for the remainder of this manuscript these gels will be referred to as 100 %, 99 % and 95 % respectively.

2.2. Degradation Studies.

Degradation studies were performed at 37 ^{o}C and 5 % CO_2. Wash steps on hydrogels were performed every day in either complete hMSC culture medium or phosphate-buffered saline (PBS). Culture medium or PBS was pipetted at each wash step to hydrogel-containing vials under sterile conditions. All media or PBS was then removed prior to weighing, and the next wash step was then performed.

2.3 Transmission Electron Microscopy (TEM).

100 %, 99 % and 95 % gels were imaged in a JEOL JEM-2100, 200 kV transmission electron microscope equipped with two Gatan digital CCD cameras for widefield or high-resolution imaging - a Gatan Orius S200D (2k x 2k) and a Gatan Orius SC1000A (4k x 2.5k). 4 µL gel samples were placed onto carbon coated 300-mesh copper grids (ProSciTech, Queensland, Australia) after they had been glow discharged (Emitech k950x with k350 attachment). Excess fluid was drawn off, and the samples were negatively stained with two drops of uranyl acetate, wicking away excess after each. The samples were then allowed to dry at room temperature before visualisation in the TEM.

A statistical analysis on the collated images was conducted through the freely available statistical analysis program, FiberApp[51]. Fibrillar characteristics of interest explored as part of this analysis included fiber width, length, periodicity of helical fibers, and persistence lengths.

2.4 Rheology.

Samples were submitted to rheological tests (Physica MCR 301 Anton Paar, Rheometer) to determine the storage modulus (G') and loss modulus (G'') of the gels. The measurements were performed using a parallel plate geometry (25 mm disk) with a 0.25 mm gap at 37 ^{o}C. Oscillatory measurements were performed either at constant frequency (1 Hz) over 300 seconds, or in a frequency sweep 0.1-100 Hz. All samples were run in triplicate and the data plotted as a mean value ± one standard deviation. The 95 % gels were too fragile to be transferred to the rheometer and therefore unable to be measured.

2.5 Small Angle X-ray Scattering (SAXS).

Small Angle X-ray Scattering (SAXS) experiments were performed at room temperature on the SAXS / WAXS beamline at the Australian Synchrotron. The three peptide assemblies (100 %, 99 % and 95 % gels) were prepared in dilute solutions to prevent gelation (0.5 mg/mL) in Milli-Q® (MQ) water and left to equilibrate for 24 hours at room temperature. 100 µl of each assembly was loaded into a 96-well plate held on a robotically controlled x-y stage, and transferred to the beamline via a quartz capillary connected to a syringe pump. The experiments used a beam wavelength of λ = 1.03320 Å^{-1} (12.0 keV) with dimensions of 300 μm × 200 μm and a typical flux of 1.2 × 10^{13} photons per second. 2D diffraction images were collected on a Pilatus 1M detector at *q*-ranges between 0.02 and 0.25 Å^{-1}. Spectra were recorded under flow (0.15 mL/min) to prevent x-ray damage from the beam. Multiples of approximately 15 spectra were recorded for each time point (exposure time = 1 second) and averaged spectra are shown after background subtraction against MQ water in the same capillary.

2.6 Cell Culture.

Human bone-marrow derived mesenchymal stem cells (hMSCs, Lonza, PT-2501, Basel, Switzerland), were cultured for seeding upon 100 %, 99 % and 95 % gels, and to observe overall viability.

A complete hMSC culture medium was formed from Dulbecco's Modified Eagles' Medium (DMEM – low glucose) (Sigma-Aldrich, St Louis, USA), foetal bovine serum (10 % - 12003C-500 mL, Sigma-Aldrich, St Louis, USA), HEPES (15 mM, purity ≥ 99.5 %, H4034-500 g, Sigma-Aldrich, St Louis, USA), L-Glutamine (2 mM, 59202C, Sigma-Aldrich, St Louis, USA), Antibiotics Penicillin-Streptomycin (1X, P4333-100 mL, Sigma-Aldrich, St Louis, USA), Epidermal Growth Factor (20 ng/mL, E9644-.2 mg, Sigma-Aldrich, St Louis, USA), and Fibroblast Growth Factor (1 ng/mL F3685-25UG, Sigma-Aldrich, St Louis, USA).

Cells were cultured in the hMSC culture medium in T-75 tissue cell culture flasks, and incubated at 37 °C in an atmosphere of humidified 5 % CO_2 / 95 % air. The media was changed every second day, until such time as the cells reached 90 % confluency and were ready for passage. Cells were used between passages 1-14 (P1-P14). Cell counting was performed under light microscopy visualisation of a haemocytometer slide (4 x 16 well grid) and the addition of Trypan Blue cell stain solution (0.4 % - 15250061, Gibco, New York, USA).

2.7 Live-Dead Cell Assay.

A Live-Dead Cell Staining Kit (04511-1KT-F, Sigma Aldrich, Melbourne, Australia) was used for simultaneous fluorescence staining of viable and dead cells. The stain kit contains Calcein-AM (which is converted to a highly fluorescent molecule by metabolically active cells) and Propidium Iodide (PI) (which stains the DNA of dead or dying cells).

Cells were collected and seeded at 36,000 cells/mL into a 24 well plate. After 24 hours incubation, the cells were washed twice in PBS (15 minutes) before incubating the cells within a stain solution of Calcein AM and PI, in PBS for 60 minutes. Samples were then washed twice more in PBS (15 minutes) before imaging on a dual channel fluorescent microscope.

2.8 Fluorescence Microscopy.

Imaging was performed using the Olympus IX81 fluorescence microscope (Olympus, Tokyo, Japan) and images were captured using Olympus Dimension Cellsens software (Olympus, Tokyo, Japan). Fluorescein / Green fluorescent protein / Alexa Fluor 488 (FITC / GFP / AF488), and Tetramethylrhodamine-isothiocyanate / Alexa Fluor 568 (TRITC / AF568) were used as dual band filter channels to capture fluorescence from live and dead cells respectively. A Sigma-Aldrich Live-Dead Cell Staining Kit (04511-1KT-F, St Louis, USA) was utilised for simultaneous fluorescence staining of viable and dead cells, with excitation of both stains (Calcein-AM and Propidium Iodide) induced at 490 nm, and emission wavelengths captured at 518 nm (FITC), and 580 nm (TRITC) respectively.

2.9 Presto Blue Cell Viability Assay.

500 μL 100 %, 99 % and 95 % gels were formed in black 96-well MicroWell immunoplates (Nunc, Roskilde, Denmark), and incubated for 24 hours. Gels were then washed extensively with hMSC media, and seeded with 72,000 MSCs per well for 1,3 or 6 days, after which the gels were washed twice with PBS before incubation with the cell permeable, resazurin-based Presto Blue assay solution (Invitrogen, Carlsbad, California, USA) as per the manufacturer's recommendations. Presto Blue fluorescence was determined by a CLARIOstar Microplate Reader (BMG Labtech, Ortenberg, Germany) with excitation at 535 nm and emission 615 nm. All samples were run in triplicate and the data plotted as a mean value ± one standard deviation.

3. RESULTS & DISCUSSION.

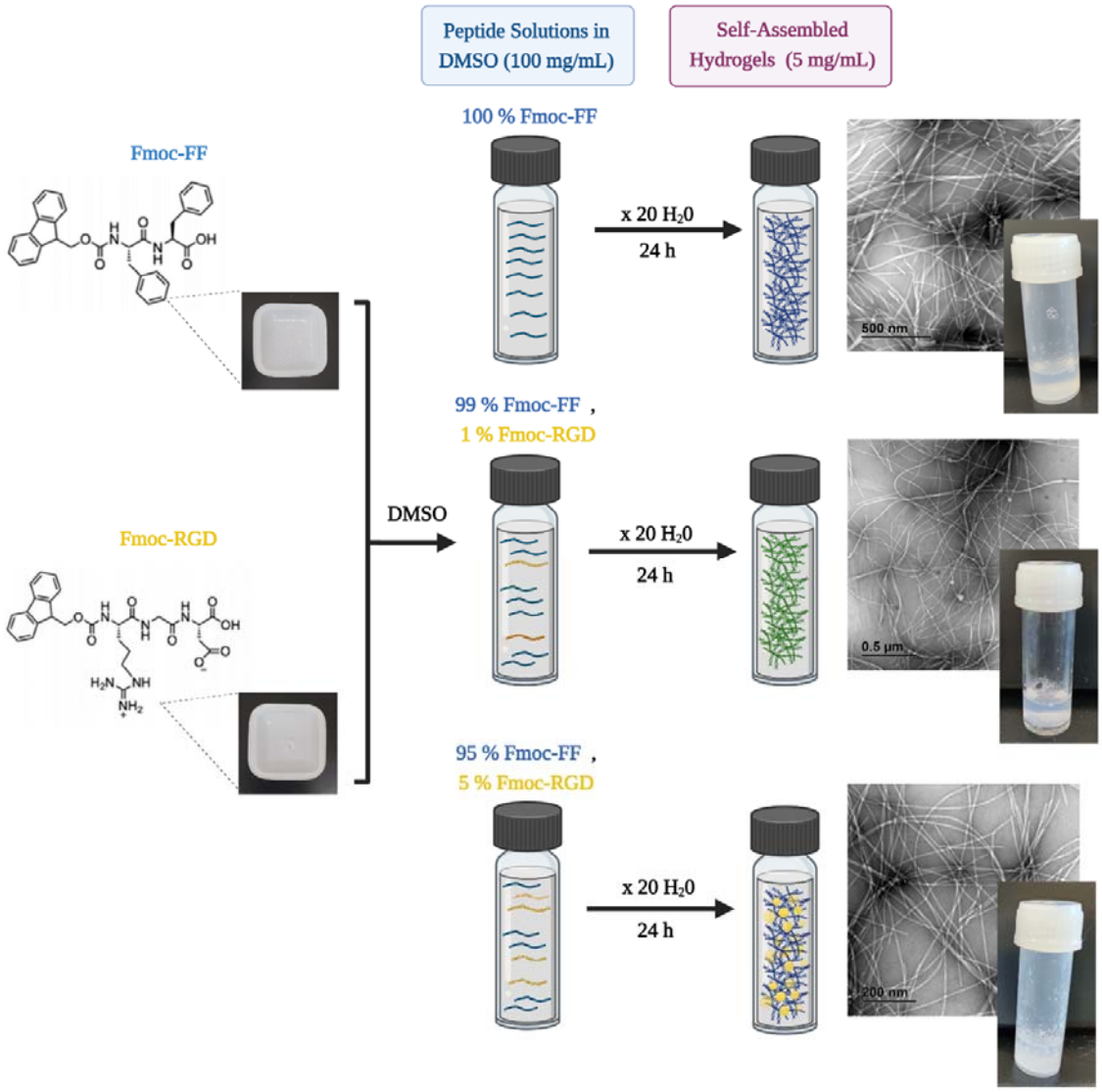

Figure 1: Stoichiometric mixing of Fmoc-FF and Fmoc-RGD in DMSO before solvent exchange into ultrapure water results in the rapid formation of viscoelastic hydrogels. TEM imaging revealed the formation of self-assembled nanofibrillar network arrangements within hydrogels of 100 %, 99 % and 95 % Fmoc-FF. Figure created with Biorender.com.

3.1 Hybrid Fmoc-FF Fmoc-RGD hydrogels degrade more rapidly than pure Fmoc-FF hydrogels.

After 24 hours all 3 systems (100 %, 99 % and 95 %) formed self-supporting hydrogels (**figure 1 and figure 2b**). Hydrogel scaffolds for tissue engineering are required to enhance cellular survival and differentiation for a finite period, before eventual degradation or resorption within the human body. Once engineered tissue is formed, scaffolds are then typically required to degrade at a desired rate to promote integration of newly formed tissue with the damaged native tissue [52]. Rates of degradation generally need to match concomitant rates of new tissue formation from the cells embedded within hydrogels [52], allowing gradual deposition and integration of engineered tissue into defect areas, and promoting remodelling of the ECM [53, 54]. The rate of scaffold degradation is known to ultimately influence the spatial organisation of cells, matrix biosynthesis, histological patterns and eventual integration of a tissue construct into surrounding tissue [54]. Collectively these factors may influence the overall viability and longevity of engineered tissue.

We set out to compare the long-term stability of 100 %, 99 % and 95 % hydrogels when subjected to media washes. We observed more rapid mass loss within hybrid gels in response to media washes at a rate up to 1.5 times greater than pure Fmoc-FF gels (**figure 2a**). Overall, the 95 % gels degrade into non-self-supporting hydrogel slurries more rapidly than the 99 % gels (**figure 2b, c** and **supplementary figures 1,2**). In DMEM, the 95 % gels had degraded to half of their initial mass within two days (**figure 2a**), whereas 100 % and 99 % gels reached this same degradation point within 32 and 36 days respectively. Similarly, in PBS, the 95 % gels degraded to half of their initial mass within two days, and 99 % gels reached this point within 38 days (**supplementary figure 1a**). 100 % gels never reached this level of degradation point over the 46-day study period, with 75 % of gel volume remaining upon study completion (**supplementary figure 1a**). These results suggest that 95 % gels are unsuitable for long term 3D cell culture applications.

Gel mass degradation appears to be the end-product of hydrolytic degradation. Within the hydrogels individual nanofibrils are held by long-range non-covalent forces such as the π- π stacking from the Fmoc protecting groups which contribute to gel stability [41]. In the presence of complex fluids such as cell culture media, these forces are more easily disrupted, speeding up degradation.

The macroscale mechanical properties of the gels were investigated by rheology, and the storage moduli (**G'**) of 100 % and 99 % Fmoc-FF gels were observed to be larger than their respective loss moduli (**G"**) (**figure 2d-e**), suggesting the gels take on the properties of a viscoelastic solid. Storage moduli for both 100 % and 99 % gels were in the region between 0.8-2 kilopascals (kPa), which is typical for soft physically crosslinked gels. In addition, rheological analysis revealed that these gels were stable under oscillatory strain up until 60 Hz and 48 Hz respectively, where they underwent an irreversible viscoelastic solid-liquid state change (**supplementary figure 3a-d**). 95 % gels were unable to be analysed due to premature dissolution.

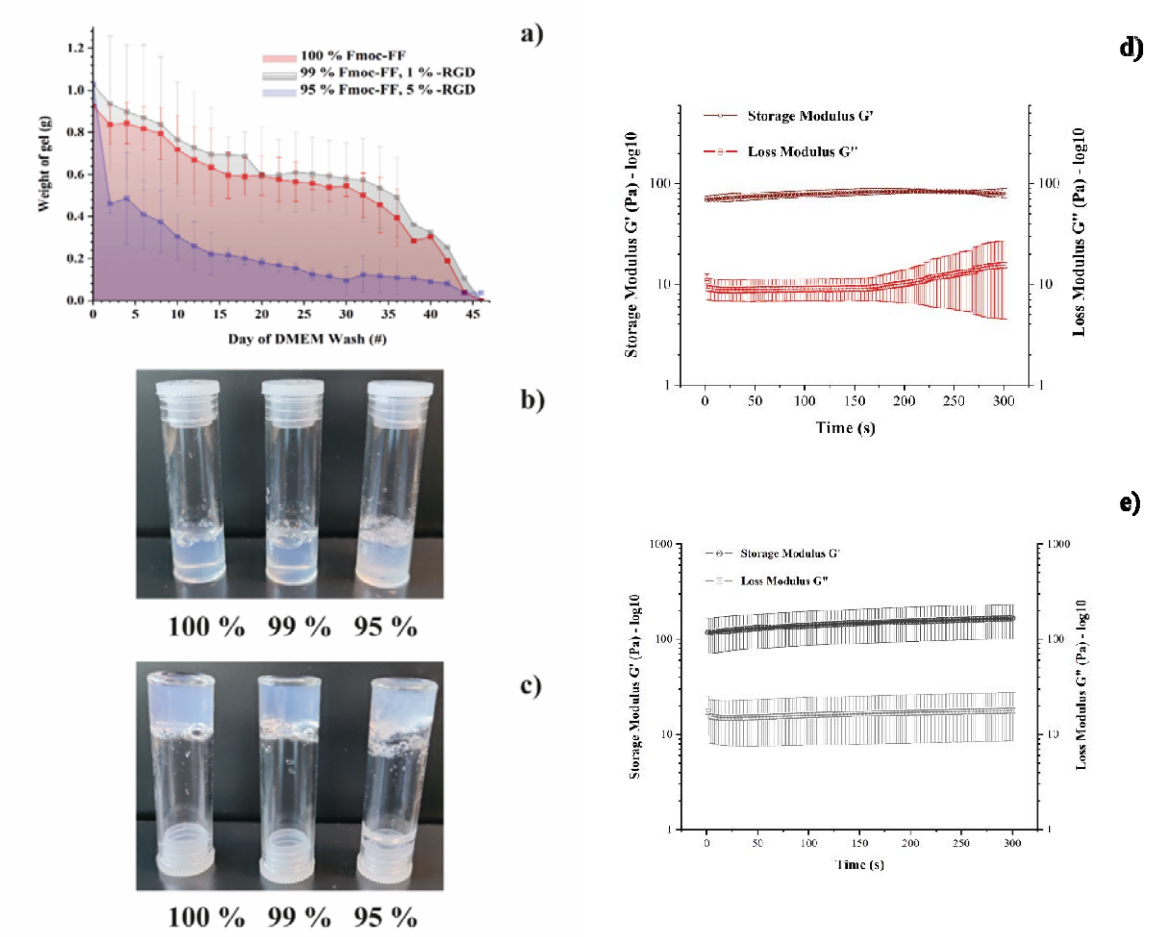

Figure 2: Rate of hydrogel degradation is affected by RGD concentration: **a)** Mass loss assays for 100 %, 99 % and 95 % gels in DMEM. Error bars denote Mean ± SD. **b)** Freshly formed self-supporting hydrogels (100 % (left), 99 % (centre) and 95 % Fmoc-FF (right)). **c)** 95 % hydrogels (right) degrade rapidly. **d-e)** Rheological characterisation of storage (G') and loss (G") moduli of **(d)** 100 % and **(e)** 99 % gels.

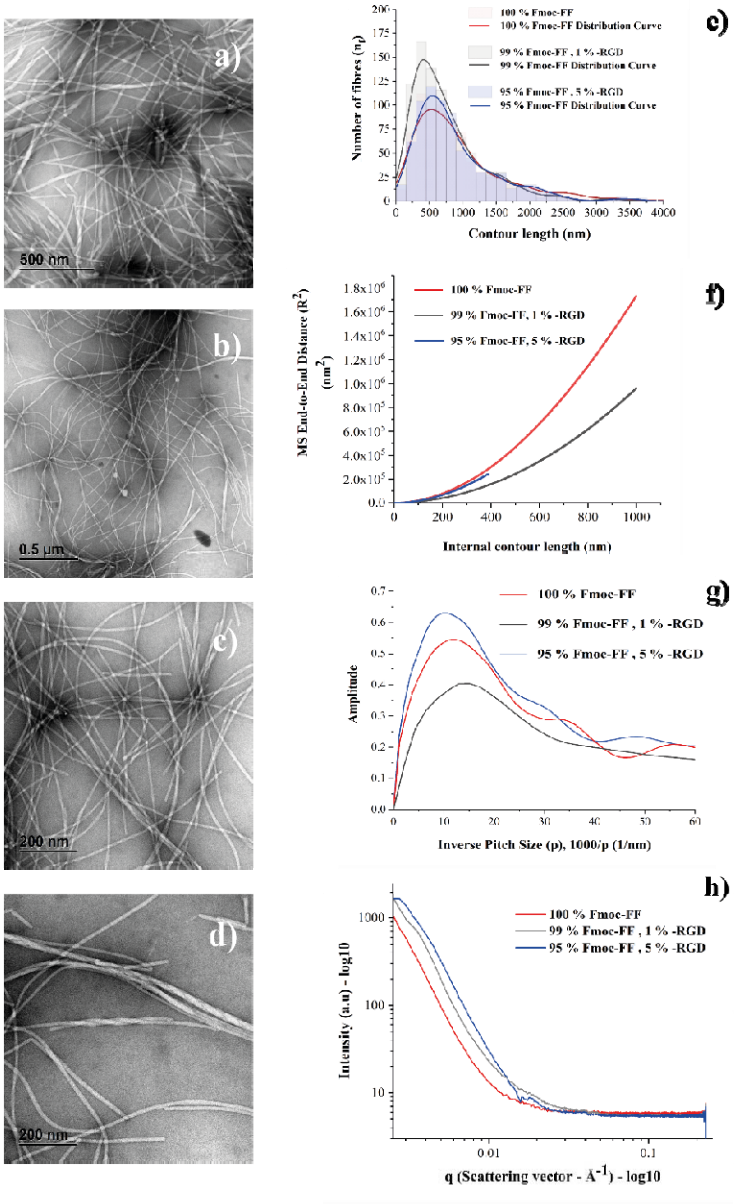

Figure 3: Biophysical analysis of the self-assembled nanofibrils reveals distinct nanoscale differences between the gels. **a-d)** TEM images of: **a)** 100 %, **b)** 99 % and **c)** 95 % gel nanofibrils. **d)** An example of the periodically twisted ribbon-like nanofibrils seen in all 3 systems (image is from the 99 % gels). **e-g)** Statistical analysis of the TEM images of the nanofibrils - all analysis performed on over 500 nanofibrils, **e)** Nanofibril contour length distribution of the three gels, **f)** Mean-square end-to-end distance of the persistence length (λ_{MSED}) of the three gels, **g)** Direct Fourier Transform (DFT) analysis of the pitch of the twisted ribbon-like nanofibrils observed, **h)** Small-angle X-ray scattering (SAXS) analysis of the three nanofibrillar samples at non-gelling concentrations.

3.2 Increasing RGD concentration reduces the stability of the resultant gels.

To further investigate the nanostructures of the nanofibrillar assemblies created by RGD incorporation, and to try to determine the cause of the premature degradation of the 95 % gels, negative stain TEM imaging of the gels was performed. TEM revealed a network of interwoven nanofibrils for all three hydrogels. Closer inspection reveals that all three nanofibrils displayed polymorphic behaviour with mixtures of linear nanofibrils, interspersed with those possessing a helical or twisted ribbon structure [55] (**figure 3a-d, supplementary figure 4**).

Quantitative analysis of the nanofibril morphology within the three gels using the freely available analysis software FiberApp[51] revealed that the nanofibrils within the 99 % hydrogels were distinct from those seen within 100 % and 95 % gels (**figures 3e-h**). Quantification of the contour length distributions of the fibrils in the 99 % gels showed that the fibrils tended to be shorter, with the mean of the 100 %, 99 % and 95 % gels being 529, 418 and 544 nm respectively (**figure 3e**). Mean square end-to-end distance (MSED) analysis of the persistence length (λ_{MSED}) of the fibers (**figure 3f**) showed that the stiffness of fibers found within 99 % gels to be less than the other two gels studied (λ_{MSED} = 3.51 µm, 1.77 µm and 2.38 µm for 100 %, 99 % and 95 % gels respectively). Discrete Fourier Transform (DFT) analysis of the periodicity of those fibers with a clear twisted ribbon architecture once again revealed the 99 % gels to be distinct from the 100 % and 95 % gels. The peak-to-peak periodicity of the 99 % gels was just 70.7 nm (from **figure 3g** - 1000/14.15 nm^{-1}), whilst this value was 87.4 nm and 93.7 nm for the 100 % gels and the 95 % gels (**figure 3g**). These findings collectively highlight that there is a distinct difference in the biophysical properties of the nanofibrils found in 99 % gels compared to the other two systems. This is most likely explained by improved incorporation of RGD ligands into the nanofibrillar structures at 99 % concentrations than at 95 % concentrations (**figure 1**).

3.3 Above a certain threshold Fmoc-RGD self-aggregates producing heterogeneous assemblies.

On a molecular level, our results suggest that at low concentrations Fmoc-RGD ligands co-assemble with the Fmoc-FF peptides producing nanofibrils that are distinct from the pure Fmoc-FF population (as depicted in **figure 1**). Once the concentration of Fmoc-RGD ligands increases past a currently unknown threshold (between 1-5 % RGD), favourable insertion of Fmoc-RGD into the assembling nanofibrils is lost, and we hypothesise that instead the Fmoc-RGD ligands non-specifically aggregate into unstructured colloidal assemblies, leaving behind a network of nanofibrils similar to that of the pure Fmoc-FF solution (**figure 1**). The presence of the proposed aggregated Fmoc-RGD colloids now reduces the long-range order of the nanofibrils formed, preventing the complete gelation of the 95 % samples. Similar phenomena have been observed when adding polysaccharides to Fmoc derived self-assembling peptides, where the gels can incorporate low concentrations of polysaccharide and behave similarly to the pure peptide gels, but at higher concentrations the non-assembling behaviour of the polysaccharide begins to dominate [56].

This hypothesis is backed up by small angle X-ray scattering (SAXS) data (**figure 3h**) which shows that the pure 100 % Fmoc-FF fibers and the 99 % fibers have form factors with a slope approximating q^{-1} indicative of long rod-like structure (nanofibrils) formation. For these two assemblies the intensity of scattering continues to increase exponentially past the low scattering vector (q) limit of these plots (~ 0.002 $Å^{-1}$) due to the contour length of the fibrils being much larger than can be detected at q_{min} (or D_{max} in non-reciprocal space – NB: $q = \frac{2\pi}{D}$, therefore D_{max} ~ 314 nm).

The 95 % fibers, whilst still being dominated by this rod-like form factor (still with an abundance of nanofibrils), start to plateau at low q. This plateau is likely indicative of the beginning of a Guinier region and the presence of smaller amorphous aggregates of Fmoc-RGD that do not exceed d_{max}. However, it should be noted that the size of this apparent Guinier region was too small to perform a reasonable analysis of the radius of gyration (Rg) of these amorphous aggregates, this is likely due to the heterogeneous nature (fibrils plus aggregates) of the 95 % gels.

3.4 RGD concentration affects MSC viability in hydrogels over time.

We next examined the viability of MSCs cultured within the three gels. Live-dead assays (**figure 4a-c**) revealed that a majority of cells cultured in each of the gels remained viable after 24 hours following seeding onto gels. As previously observed [57, 58], this suggests that Fmoc-FF based hydrogels are suitable for MSC culture. Moreover, the fluorescent microscopy analysis showed similar results to the degradation studies, and showed that even after 24 hours the structural integrity of 95 % gels was impaired. Repeated images show non-continuous gels broken into small fragments (**figure 4c**), that whilst still able to support viable MSCs, these did not remain in a self-supporting hydrogel structure. This again highlights their unsuitability for long term cell culturing applications.

A resazurin based viability (Presto Blue™) assay showed statistically similar levels of cell viability between 100 % and 99 % over 6 days. The 99 % gels only showed slightly greater fluorescence (7-fold increase - **figure 4d**) after 6 days when compared to 100 % gels (4-fold increase - **figure 4d**), and thus highlighted similar levels of cell growth in the two gel types.

By contrast, 95 % gels showed a high amount of metabolic activity (compared with the 99 % and 100 % gels) after one day, which is likely due to the high concentrations of RGD ligands within the hydrogels. However, after three days, the metabolic activity dropped to baseline levels. This is likely due to premature degradation of the 95 % gels. With exposure to repeated media washes, much of the semi-degraded gel was washed away, along with the cells encapsulated in those gel fragments (**figure 4d**). This loss of cells due to repeated washes and increased gel degradation likely explains the apparent drop in cell number after one day in the 95 % gels.

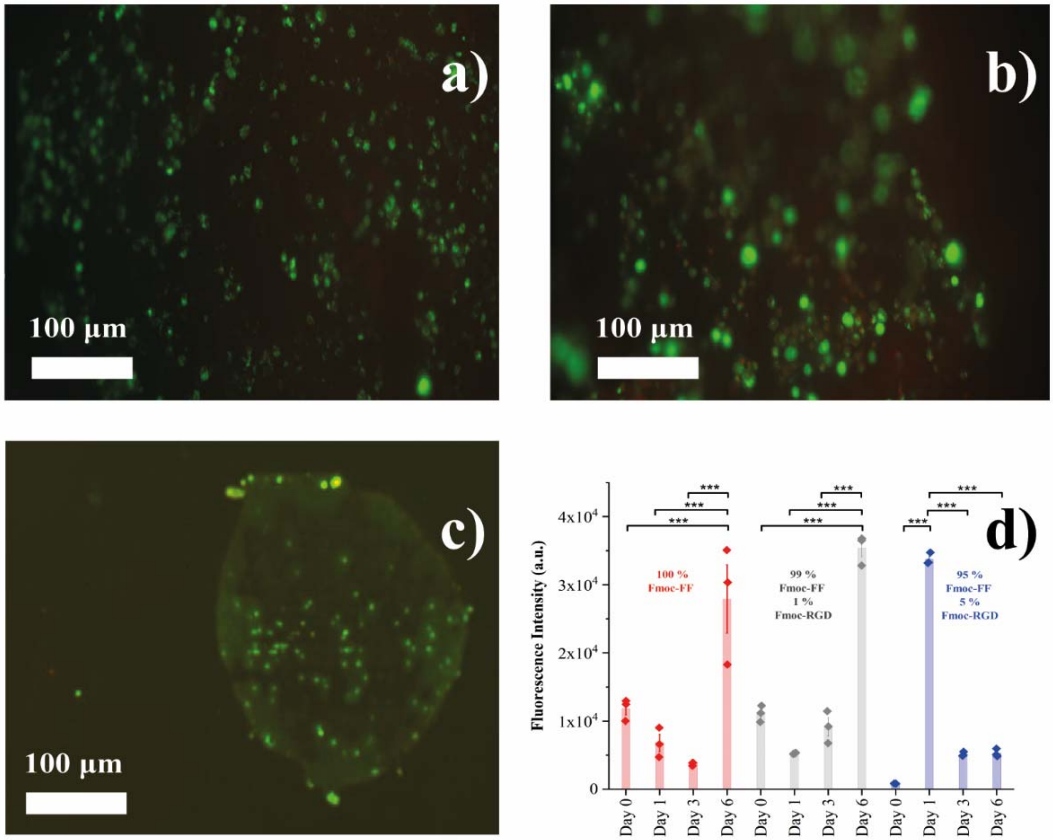

Figure 4: RGD concentration affects MSC growth over 6 days. Live-dead assays of mesenchymal stem cells (MSCs) seeded upon **(a)** 100 %, **(b)** 99 % and **(c)** 95 % hydrogels after 24 hours culture. Cells were stained with calcein AM (green) and propidium iodide (red). **(d)** Resazurin based metabolic activity assay (PrestoBlue™) on the 3 gels studies, error bars show ± 1 Standard Deviation. *** = P <0.001.

4. CONCLUSION

Tissue engineering requires suitable materials which can behave as *in vitro* scaffolds or implantable biomaterials. To fulfil these actions, biomaterials such as hydrogels must have a capacity to support cells for a finite period to achieve proliferation and maturation, before undergoing subsequent degradation at a rate which matches that of tissue growth. Fmoc-FF, and hybrid Fmoc-FF-RGD hydrogels demonstrate potential to meet these challenges through their ability to support MSC viability, with 99 % Fmoc-FF, 1 % Fmoc-RGD gels increasing overall MSC growth by up to 7 times whilst undergoing relatively slow degradation. Further, we correlated gel degradation patterns to show that the 95 % Fmoc-FF, 5 % Fmoc-RGD gels degrade significantly quicker than pure Fmoc-FF gels demonstrating that gel stability is inherently linked to RGD content, with greater quantities of RGD contributing to more unstable hydrogels that cannot support the long term culture of MSCs. Through TEM imaging, nanofibrillar statistical analysis and SAXS measurements, we proposed a molecular explanation for the reduction in gel stability at high RGD concentrations. At lower concentrations of RGD, the Fmoc-RGD peptides preferentially co-aggregate with the Fmoc-FF peptides forming hybrid nanofibrils that possess subtly different architectures to the pure Fmoc-FF fibrils. At higher RGD concentrations, RGD is no longer incorporated into the growing nanofibrils and instead has a preference to self-aggregate into non-fibrillar colloidal assemblies, with the remaining nanofibrils returning to a morphology resembling pure 100 % Fmoc-FF fibrils. This colloidal heterogeneity in the 95 % gels explains the incomplete gelation and premature degradation of these hydrogels. The results from this work should assist biomaterials scientists and tissue engineers in the rational design of 3D scaffolds that contain optimal concentrations of bioactive ligands, such as RGD, to promote biological responses without compromising the integrity and biophysical properties of the fabricated hydrogels.

Acknowledgements

NPR would like to acknowledge the La Trobe Institute of Molecular Sciences (LIMS) for the receipt of a Nicholas Hoogenraad fellowship in Molecular Sciences, and Dr. Susi Seibt for assistance on the SAXS / WAXS beamline at the Australian Synchrotron. This research was undertaken, in part, on this beamline at the Australian Synchrotron, part of ANSTO.

REFERENCES

1. Safiri, S., et al., Global, regional and national burden of osteoarthritis 1990-2017: a systematic analysis of the Global Burden of Disease Study 2017. *Annals of the Rheumatic Diseases* **2020,** *79*, 819-828.

2. Hunter, D. J.; Bierma-Zeinstra, S., Osteoarthritis. *Lancet* **2019,** *393*, 1745-1759.

3. Atkinson, H. D. E., The negatives of knee replacement surgery: complications and the dissatisfied patient. *Orthopaedics and Trauma* **2017,** *31* (1), 25-33.

4. Pastides, P.; Chimutengwende-Gordon, M.; Maffulli, N.; Khan, W., Stem Cell Therapy for Human Cartilage Defects: A Systematic Review. *Osteoarthritis and cartilage / OARS, Osteoarthritis Research Society* **2013,** *21*.

5. Chimutengwende-Gordon, M., et al., Stem cell transplantation for the treatment of osteochondral defects of the knee: Operative technique for a single-stage transplantation procedure using bone marrow-derived mesenchymal stem cells. *The Knee* **2020,** *28*.

6. Hildner, F., et al., State of the art and future perspectives of articular cartilage regeneration: a focus on adipose-derived stem cells and platelet-derived products. *Journal of Tissue Engineering and Regenerative Medicine* **2011,** *5* (4), e36-e51.

7. O'Sullivan, J., et al., Mesenchymal chondroprogenitor cell origin and therapeutic potential. *Stem Cell Research & Therapy* **2011,** *2*, 8.

8. Osborne, H., et al., Australasian College of Sports Physicians—position statement: the place of mesenchymal stem/stromal cell therapies in sport and exercise medicine. *British Journal of Sports Medicine* **2016,** *50* (20), 1237.

9. Lee, K., et al., A Patch of Detachable Hybrid Microneedle Depot for Localized Delivery of Mesenchymal Stem Cells in Regeneration Therapy. *Advanced Functional Materials* **2020,** *30*, 2000086.

10. Kehoe, O., et al., Intra-articular injection of mesenchymal stem cells leads to reduced inflammation and cartilage damage in murine antigen-induced arthritis. *Journal of Translational Medicine* **2014,** *12* (1), 157.

11. Diekman, B. O., et al., Intra-articular delivery of purified mesenchymal stem cells from C57BL/6 or MRL/MpJ superhealer mice prevents posttraumatic arthritis. *Cell Transplant* **2013,** *22* (8), 1395-408.

12. Mak, J., et al., Intra-articular injection of synovial mesenchymal stem cells improves cartilage repair in a mouse injury model. *Sci Rep* **2016,** *6*, 23076.

13. Pak, J.; Chang, J. J.; Lee, J. H.; Lee, S. H., Safety reporting on implantation of autologous adipose tissue-derived stem cells with platelet-rich plasma into human articular joints. *BMC Musculoskelet Disord* **2013,** *14*, 337.

14. Peeters, C. M., et al., Safety of intra-articular cell-therapy with culture-expanded stem cells in humans: a systematic literature review. *Osteoarthritis Cartilage* **2013,** *21* (10), 1465-73.

15. Abdulghani, S.; Morouço, P. G., Biofabrication for osteochondral tissue regeneration: bioink printability requirements. *J Mater Sci Mater Med* **2019,** *30* (2), 20.

16. Zhu, T., et al., Engineered three-dimensional scaffolds for enhanced bone regeneration in osteonecrosis. *Bioact Mater* **2020,** *5* (3), 584-601.

17. Zhang, Q.; Lu, H.; Kawazoe, N.; Chen, G., Pore size effect of collagen scaffolds on cartilage regeneration. *Acta Biomaterialia* **2014,** *10* (5), 2005-2013.

18. Qi, Y., et al., The restoration of full-thickness cartilage defects with mesenchymal stem cells (MSCs) loaded and cross-linked bilayer collagen scaffolds on rabbit model. *Mol Biol Rep* **2012,** *39* (2), 1231-7.

19. Correia, C. R., et al., Chitosan Scaffolds Containing Hyaluronic Acid for Cartilage Tissue Engineering. *Tissue Engineering Part C: Methods* **2011,** *17* (7), 717-730.

20. Yamane, S., et al., Feasibility of chitosan-based hyaluronic acid hybrid biomaterial for a novel scaffold in cartilage tissue engineering. *Biomaterials* **2005,** *26* (6), 611-619.

21. Yoo, H. S.; Lee, E. A.; Yoon, J. J.; Park, T. G., Hyaluronic acid modified biodegradable scaffolds for cartilage tissue engineering. *Biomaterials* **2005,** *26* (14), 1925-1933.

22. Lee, C., et al., Human articular cartilage repair: Sources and detection of cytotoxicity and genotoxicity in photo-crosslinkable hydrogel bioscaffolds. *Stem Cells Transl Med* **2020,** *9* (3), 302-315.

23. Kim, I. L.; Mauck, R. L.; Burdick, J. A., Hydrogel design for cartilage tissue engineering: A case study with hyaluronic acid. *Biomaterials* **2011,** *32* (34), 8771-8782.

24. Hoshiba, T.; Lu, H.; Kawazoe, N.; Chen, G., Decellularized matrices for tissue engineering. *Expert Opin Biol Ther* **2010,** *10* (12), 1717-28.

25. Reddy, M. S. B.; Ponnamma, D.; Choudhary, R.; Sadasivuni, K. K., A Comparative Review of Natural and Synthetic Biopolymer Composite Scaffolds. *Polymers* **2021,** *13*, 1105.

26. Li, Y.; Rodrigues, J.; Tomás, H., Injectable and biodegradable hydrogels: gelation, biodegradation and biomedical applications. *Chemical Society Reviews* **2012,** *41* (6), 2193-2221.

27. Spicer, C. D., Hydrogel scaffolds for tissue engineering: the importance of polymer choice. *Polymer Chemistry* **2020,** *11* (2), 184-219.

28. Mamsen, F. P., et al., Differences of embedding adipose-derived stromal cells in natural and synthetic scaffolds for dermal and subcutaneous delivery. *Stem Cell Research & Therapy* **2021,** *12* (1), 68.

29. Reynolds, N. P., Amyloid-like peptide nanofibrils as scaffolds for tissue engineering: Progress and challenges *Biointerphases* **2019,** *14*, 040801.

30. Wei, G., et al., Self-assembling peptide and protein amyloids: from structure to tailored function in nanotechnology. *Chemical Society Reviews* **2017,** *46* (15), 4661-4708.

31. Orbach, R., et al., The Rheological and Structural Properties of Fmoc-Peptide-Based Hydrogels: The Effect of Aromatic Molecular Architecture on Self-Assembly and Physical Characteristics. *Langmuir* **2012,** *28* (4), 2015-2022.

32. Smith, A. M., et al., Fmoc-Diphenylalanine Self Assembles to a Hydrogel via a Novel Architecture Based on π–π Interlocked β-Sheets. *Advanced Materials* **2008,** *20* (1), 37-41.

33. Jayawarna, V., et al., Introducing chemical functionality in Fmoc-peptide gels for cell culture. *Acta Biomater* **2009,** *5* (3), 934-43.

34. Mahler, A., et al., Rigid, Self-Assembled Hydrogel Composed of a Modified Aromatic Dipeptide. *Advanced Materials* **2006,** *18* (11), 1365-1370.

35. Reynolds, N. P.; Charnley, M.; Mezzenga, R.; Hartley, P. G., Engineered Lysozyme Amyloid Fibril Networks Support Cellular Growth and Spreading. *Biomacromolecules* **2014,** *15* (2), 599-608.

36. Reynolds, N. P., et al., Nanotopographic Surfaces with Defined Surface Chemistries from Amyloid Fibril Networks Can Control Cell Attachment. *Biomacromolecules* **2013,** *14* (7), 2305-2316.

37. Reynolds, N. P., et al., Biomimetic Topography and Chemistry Control Cell Attachment to Amyloid Fibrils. *Biomacromolecules* **2015,** *16* (5), 1556-1565.

38. Gilbert, J., et al., Chitosan-coated amyloid fibrils increase adipogenesis of mesenchymal stem cells. *Materials Science and Engineering: C* **2017,** *79*, 363-371.

39. Das, S., et al., Implantable amyloid hydrogels for promoting stem cell differentiation to neurons. *NPG Asia Materials* **2016,** *8* (9), e304-e304.

40. Diaferia, C.; Morelli, G.; Accardo, A., Fmoc-diphenylalanine as a suitable building block for the preparation of hybrid materials and their potential applications. *Journal of Materials Chemistry B* **2019,** *7* (34), 5142-5155.

41. Zhou, M., et al., Self-assembled peptide-based hydrogels as scaffolds for anchorage-dependent cells. *Biomaterials* **2009,** *30* (13), 2523-30.

42. Wang, Y. L., et al., Self-Assembled Peptide-Based Hydrogels as Scaffolds for Proliferation and Multi-Differentiation of Mesenchymal Stem Cells. *Macromol Biosci* **2017,** *17* (4).

43. Bellis, S. L., Advantages of RGD peptides for directing cell association with biomaterials. *Biomaterials* **2011,** *32* (18), 4205-4210.

44. MacPherson, D.; Bram, Y.; Park, J.; Schwartz, R. E., Peptide-based scaffolds for the culture and maintenance of primary human hepatocytes. *Scientific Reports* **2021,** *11*, 6772.

45. Zhou, X., et al., Improved Human Bone Marrow Mesenchymal Stem Cell Osteogenesis in 3D Bioprinted Tissue Scaffolds with Low Intensity Pulsed Ultrasound Stimulation. *Scientific Reports* **2016,** *6*, 32876.

46. Schuh, E., et al., The influence of matrix elasticity on chondrocyte behavior in 3D. *Journal of Tissue Engineering and Regenerative Medicine* **2012,** *6*, e31-e42.

47. Leach, J. K.; Whitehead, J., Materials-Directed Differentiation of Mesenchymal Stem Cells for Tissue Engineering and Regeneration. *ACS Biomater Sci Eng* **2018,** *4* (4), 1115-1127.

48. Faia-Torres, A. B., et al., Osteogenic differentiation of human mesenchymal stem cells in the absence of osteogenic supplements: A surface-roughness gradient study. *Acta Biomaterialia* **2015,** *28*, 64-75.

49. Faia-Torres, A. B., et al., Differential regulation of osteogenic differentiation of stem cells on surface roughness gradients. *Biomaterials* **2014,** *35* (33), 9023-9032.

50. Faia-Torres, A. B., et al., Regulation of Human Mesenchymal Stem Cell Osteogenesis by Specific Surface Density of Fibronectin: a Gradient Study. *ACS Applied Materials & Interfaces* **2015,** *7* (4), 2367-2375.

51. Usov, I.; Mezzenga, R., FiberApp: An Open-Source Software for Tracking and Analyzing Polymers, Filaments, Biomacromolecules, and Fibrous Objects. *Macromolecules* **2015,** *48* (5), 1269-1280.

52. Willerth, S. M.; Sakiyama-Elbert, S. E., Combining Stem Cells and Biomaterial Scaffolds for Constructing Tissues and Cell Delivery. *StemJournal* **2019,** *1*, 1-25.

53. Bao, W., et al., Advancements and Frontiers in the High Performance of Natural Hydrogels for Cartilage Tissue Engineering. *Frontiers in Chemistry* **2020,** *8* (53), 1.

54. Toh, W. S.; Lim, T. C.; Kurisawa, M.; Spector, M., Modulation of mesenchymal stem cell chondrogenesis in a tunable hyaluronic acid hydrogel microenvironment. *Biomaterials* **2012,** *33* (15), 3835-45.

55. Reynolds, N. P., et al., Competition between crystal and fibril formation in molecular mutations of amyloidogenic peptides. *Nature communications* **2017,** *8*, 1-10.

56. Firipis, K., et al., Tuneable Hybrid Hydrogels via Complementary Self-Assembly of a Bioactive Peptide with a Robust Polysaccharide. *ACS Biomaterials Science & Engineering* **2021,** *7* (7), 3340-3350.

57. Li, Z., et al., Effects of RGD nanospacing on chondrogenic differentiation of mesenchymal stem cells. *Journal of Materials Chemistry B* **2015,** *3* (26), 5197-5209.

58. Wang, J., et al., Biodegradable Polymer Membranes Applied in Guided Bone/Tissue Regeneration: A Review. *Polymers* **2016,** *8*.